Journal of the Korean Nuclear Society
Volume 16, Number 2, June, 1984

Development of the LMFBR Accident Analysis Computer Code

Hee Cheon No
Korea Advanced Institute of Science and Technology
(Received August 12, 1983)

고속증식로 사고분석 코드의 개발

노 희 천
한국과학기술원
(1983. 8. 12 접수)

Abstract

Mathematically-rigorous time-volume averaged conservation equtaions were simplified to established the differential equatrons of THERMIT-6S, which is a two-fluid 3-D code. The difference equations of THERMIT-6S were obtained by discretizing the proceeding set of differential equations. The spatial discretization is characterized by a first-order spatial scheme, donor cell method, and staggered mesh layout. For time discretization, a first order semi-implicit scheme treats implictly sonic terms and terms relating to local transport phenomena and explicitly convective terms. The results were linearized by the Newton-Raphson method. In order to construct the reduced pressure equation, the linearized equations were manipulated so that all variables are coupled between mesh cells through only the pressure variable. By simulating numerically the OPERA-15 experiment, it was found that THERMIT-6S is a very powerful code in predicting reactor behavior after sodium boiling including flow coastdown, reversal flow and flow oscillation.

요 약

2상유동을 해석하기 위한 3차원 코드인 THERMIT-6S의 미분 방정식을 세우기 위해, 수학적으로 정확하게 유도된 시간과 공간에 대해 평균한 보존 방정식을 단순화했다. 미분 방정식을 불연속화(discretization)하여 THERMIT-6S의 차분방정식을 얻는다. First-order spatial scheme, donor cell method, 그리고, staggered mesh layout을 써서 공간에 대한 불연속화를 한다. 그리고 시간에 대한 불연속화는 first-order semi-implicit scheme으로써, sonic terms와 국부적인 전달 현상에 관계되는 항들은 implicit하게 그리고 대류 전달 항들은 explicit하게 취급한다. 이렇게 얻어진 방정식들은 Newton-Raphson 방법으로 선형화된다. 축소된 압력 방정식을 만들기 위해 모든 변수들이 mesh cells사이에서 단지 압력 변수를 통해서만 결부되도록, 선형화된 방정식들을 처리한다. OPERA-15 실험을 수치해석적으로 모의실험하여 본결과, THERMIT-6S가 flow coastdown, 역류, 유체진동(flow oscillation) 등을 포함하고, sodium boiling 후의 원자로내의 변화를 예측하는데 매우 유효하다는 것이 밝혀졌다.

1. Introduction

The growing public concern about the nuclear industry places an increasingly large emphasis on the safety aspects of nuclear reactors. In order to offer sufficient safety margins to assure that the public risk will be acceptably low, the U.S. Fast Breeder Reactor Safety program appoach is to provide four levels of protection, which are mainly aimed at reducing both the probability and consequences of a Core Disruptive Accident (CDA). These levels of protection are referred to as Lines of Assurance (LOA).

The present work is related to LOA 2. which in general requires an understanding of the mechanisms and design conditions which enable potential accidents to be terminated with limited core damage. Specifically the objective of this work is to develope an understanding of the role multidimensional and non-equilibrium effects of sodium boiling in determining the sequence of events during various accidents.

The first code to analyze voiding in the LMFBR was the Transfugue-1 (1) which used a homogeneous equilibrium model and a momentum integral method (2). This code was the forerunner of SAS-1A (3). The Transfugue-II code (4). an improvement of Transfugue-I, included sectional compressibility, variable vapor denities but time steps determined by the sonic velocity of the homogeneous equilibrium two-phase flow.

A series of SAS codes of ANL represent a long developed from the single-channel SAS 1A version through SAS 2A (5), SAS 3A (6), SAS 3D (7), and SAS 4A (8) which is now under development. SAS 1A was a single-channel code that included point kinetics and a combination of slip two-phase flow and single-bubble slug-boiling models. The sodium boilng model was later completly rewritten as a multibubble slug-boiling model for the multichannel SAS 2A version. SAS 3A, an expanded version of SAS 2A, contained models to allow complete calculations of cladding and fuel motions. SAS 3D used the same models as SAS 3A but restructured the code for better numerical efficiency. SAS's main limitations are the restriction from a slug model, its lack of a mixing model, and its inability to adequately incorpoate the radial heat losses and the multidimensional effect of voiding.

The BLOW code (9) developed in Germanny uses a multibubble slug-boiling model, which is similar to that in SAS 3A, in order to describe sodium voiding phenomena. The main difference between BLOW and SAS is as follcws: while the vapor velocity along a bubble can be obtained by solving the vapor mometum equation, the liquid film velocity in BLOW is directly calculated on a basis of the assumption of an universal velocity profile across the liquid film thickness.

The COBRA-3A code (10) is a homogenous equilibrium code with models such as turbulent mixing and wire-wrap mixing on a subchannel basis. The subchannel model network allowed for radial as axial sodium voiding and temperature distribution. A major limitation of COBRA-3M is its lack of capability to consider flow reversal, recirculation, and a pressure-pressure boundary condition. To provide capabilities, an ACE method scheme was developed for the COBRA-IV code (11); a temporally explicit transient pressure-velocity was selected which imposed no restriction on flow velocity and could accept either flow or pressure boundary conditions. However, this code retains a limitation of a homogeneous equilibrium model.

The main features of the BACCHUS code (12) developed at Grenoble are similar to those of COBRA-3M; the homogeneous equilibrium model, matching technigue, and mixing model.

Their main differences are that the BACCHUS uses the porous body analysis and the assumption that the flow is steady. A transient version is now under development.

Limitations of the codes are attibuted to the characteristics of sodium and of the LMFBR such as the high density ratio of liquid to vapor, the existence of the highly subcooled region, reversed flow,and sharp radial temperature gradients.

The high density ratio induces high slip between liquid and vapor and, as a result, eliminates the possibility of existence of a highly subcooled region in the bundle of the LMFBR, where vapor is condensed, causes numerical difficulties and large pressure fluctuations. The use of the equilibrium approach, in which vapor must be completely condensed in the subcooled region, enlarges pressure fluctuations and in turn numerical difficulties. The non-equilibrium approach instead of the equilibrium approach is better suited to represent real situations. Correlations for slip in annular or reversed flow are not not readily available. Hence, the slip model is avoided in the present work. Sharp radial temperature gradients and multi-dimensional voiding behavior lead us to favor a multi-dimensional model. A 3-D model is chosen because it can be transformed into 1-D or 2-D models.

According to the above brief review, a two-fluid 3-D model is selected for the analysis of sodium boiling in the LMFBR. The THERMIT code (13) is taken as the basic tool for the development of a two-fluid 3-D code due to its following main features:

1. Two-fluid 3-D code
2. Advanced numeical scheme
3. General boundary conditions

2. Differential Equations of THERMIT-6S

The mathematically rigorous differential equations of two-phase flow in Ref. 14 are simplified with several assumptions in oder to derive the differential equations of THERMIT-6S. Equations (42), (51), and (73) for conservation equations, and Eqs. (77), (78), and (80) for jump conditions in Ref. 14, are used to obtain the equations of THERMIT-6S.

Conservation Equation Equations

1. Vapor Mass

$$\frac{\partial}{\partial t}(\alpha_v\rho_v)+\nabla\cdot(\alpha_v\rho_v\vec{v}_v)=\Gamma_v \tag{1}$$

2. Liquid Mass

$$\frac{\partial}{\partial t}(\alpha_l\rho_l)+\nabla\cdot(\alpha_l\rho_l\vec{v}_l)=\Gamma_l \tag{2}$$

3. Vapor Energy

$$\frac{\partial}{\partial t}(\alpha_l\rho_l e_v)+\nabla\cdot(\alpha_v\rho_v e_v\vec{v}_v)+p\nabla\cdot(\alpha_v\vec{v}_v)+p\frac{\partial\alpha_v}{\partial t}=Q_{iv}+Q_{wv} \tag{3}$$

4. Liquid Energy

$$\frac{\partial}{\partial t}(\alpha_l\rho_l e_l)+\nabla\cdot(\alpha_l\rho_l e_l\vec{v}_l)+\nabla\cdot\alpha_l(\bar{q}_l+\bar{q}_l{}^t)+p\nabla\cdot(\alpha_l\vec{v}_l)+p\frac{\partial\alpha_l}{\partial t}=Q_{il}+Q_{wl}. \tag{4}$$

5. Vapor Momentum

$$\frac{\partial}{\partial t}(\alpha_v\rho_v\vec{v}_v)+\nabla\cdot(\alpha_v\rho_v\vec{v}_v\vec{v}_v)+\alpha_v\nabla p=\Gamma_v\vec{v}_i-\vec{F}_{iv}-\vec{F}_{wv}+\alpha_v\rho_v\vec{g} \tag{5}$$

6. Liquid Momentum

$$\frac{\partial}{\partial t}(\alpha_l\rho_l\vec{v}_l)+\nabla\cdot(\alpha_l\rho_l\vec{v}_l\vec{v}_l)+\alpha_l\nabla p=\Gamma_l\vec{v}_i-\vec{F}_i-\vec{F}_{wl}+\alpha_l\rho_l\vec{g} \tag{6}$$

Jump Condition

1. Mass

$$\Gamma_v+\Gamma_l=0 : \Gamma=\Gamma_v=-\Gamma_l \tag{7}$$

2. Energy

$$Q_{iv}+Q_{il}=0 : Q_i=Q_{iv}=-Q_{il} \tag{8}$$

3. Momentum

$$\vec{F}_{iv}+\vec{F}_{il}=0 : \vec{F}_i=\vec{F}_{iv}=-\vec{F}_{il} \tag{9}$$

Here Q_i and $\vec{F}_i$ denote interfacial energy and

momentum exchange rate, per unit volume, and Q_{wv}, Q_{wl}, $\vec{F}_{wv}$, and $\vec{F}_{wl}$ are the wall heat transfer rates and wall friction force of vapor and liquid, per unit volume, respectively. Note that $\vec{v}_i$ in the above equations is different from $\vec{v}_i \cdot \vec{n}_k$ in Ref. 14.; $\vec{v}_i$ and $\vec{v}_i \cdot \vec{n}_k$ are the interfacial material velocity and displacement velocity of the interfacial surface, respectively.

For reasons involved with the selection of a difference strategy for solving these equations, momentum equations are rewritten in a non-conservative form by using mass equations. Then Eqs (5) and (6) become

$$\alpha_v\rho_v\frac{\partial\vec{v}_v}{\partial t}+\alpha_v\rho_v\vec{v}_v\cdot\nabla\vec{v}_v+\alpha_v\nabla p = \Gamma(\vec{v}_i-\vec{v}_v)-\vec{F}_i-\vec{F}_{wv}+\alpha_v\rho_v\vec{g} \quad (10)$$

$$\alpha_l\rho_l\frac{\partial\vec{v}_l}{\partial t}+\alpha_l\rho_l\vec{v}_l\cdot\nabla\vec{v}_l+\alpha_l\rho_l\vec{v}_l\cdot\nabla\vec{v}_l+\alpha_l\nabla p = -\Gamma(\vec{v}_i-\vec{v}_l)+\vec{F}_i-\vec{F}_{wl}+\alpha_l\rho_l\vec{g} \quad (11)$$

If we assume that $\vec{v}_i$ is equal to $\vec{v}_l$, then

$$\Gamma(\vec{v}_i-\vec{v}_v)=\Gamma(\vec{v}_l-\vec{v}_v)$$
$$\Gamma(\vec{v}_i-\vec{v}_l)=0$$

In THERMIT-6S $\vec{F}_i$ consists of two components: the standard drag force ($\vec{F}_s$) and virtual mass force ($\vec{F}_v$), per unit volume. Both terms are defined as follows

$$\vec{F}_s\equiv K(\vec{v}_v-\vec{v}_l) \quad (12)$$

$$\vec{F}_v\equiv\alpha_v\rho_vC_v\left\{\frac{\partial\vec{v}_v}{\partial t}-\frac{\partial\vec{v}_l}{\partial t}+\vec{v}_v\cdot\nabla(\vec{v}_v-\vec{v}_l)+(\vec{v}_v-\vec{v}_l)\cdot\left[(\lambda-2)\nabla\vec{v}_v+(1-\lambda)\nabla\vec{v}_l\right]\right\} \quad (13)$$

Detailed description for the virtual mass force is given in Ref. 14. Introducing Eqs (12) and (13) into Eqs (10) and (11), we get the final momentum equation used in THERMIT-6S.

$$(\alpha_v\rho_v+\alpha_v\rho_lC_v)\frac{\partial\vec{v}_v}{\partial t}-\alpha_v\rho_lC_v\frac{\partial\vec{v}_l}{\partial t}+E_v+E_{vm}+\alpha_v\nabla p = -(\Gamma+K)(\vec{v}_v-\vec{v}_l)-\vec{F}_{wv}+\alpha_v\rho_v\vec{g} \quad (14)$$

$$(\alpha_l\rho_l+\alpha_v\rho_lC_v)\frac{\partial\vec{v}_l}{\partial t}-\alpha_v\rho_lC_v\frac{\partial\vec{v}_v}{\partial t}+E_l-E_{vm}+\alpha_l\nabla p = K(\vec{v}_v-\vec{v}_l)-\vec{F}_{wl}+\alpha_l\rho_l\vec{g} \quad (15)$$

where

$$E_v=\alpha_v\rho_v\vec{v}_v\cdot\nabla\vec{v}_v \quad (16)$$

$$E_l=\alpha_l\rho_l\vec{v}_l\cdot\nabla\vec{v}_l \quad (17)$$

$$E_{vm}=\alpha_v\rho_lC_v[(\lambda-1)\vec{v}_v\cdot\nabla\vec{v}_v-(\lambda-2)\vec{v}_l\cdot\nabla\vec{v}_v-\lambda\vec{v}_v\cdot\nabla\vec{v}_l-(1-\lambda)\vec{v}_l\cdot\nabla\vec{v}_l] \quad (18)$$

Q_{iv} and Q_{il} can be divided into two components contributed by mass exchange and interfacial heat flux. These are defined as follows:

$$Q_{iv}=\frac{1}{L_a}(g_mh_{iv}+q''_{iv}) \quad (19)$$

$$Q_{il}=-\frac{1}{L_a}(g_mh_{il}+q''_{il}), \quad (20)$$

where h_{il} and h_{iv} are the enthalpy on the liquid and vapor side of the interface, respectively.
q''_{il} and q''_{iv} are the heat flux on the liquid and vapor side of the interface,
g_m and $\frac{1}{L_a}$ are the interfacial mass flux and the ratio of interfacial area to fluid volume in the control volume.

$$q''_{ik}=\langle\!\langle n_k\cdot\vec{q}_k\rangle\!\rangle_a$$
$$g_m=-\langle\!\langle\dot{m}_k\rangle\!\rangle_a,$$

where $\langle\!\langle\ \rangle\!\rangle_a$ represent a quantity which is averaged over an interface The mass exchange rate Γ can be expressed in terms of g_m and $\frac{1}{L_a}$

$$\Gamma=\frac{g_m}{L_a} \quad (21)$$

According to the jump condition with the neglected term $\langle\!\langle\bar{p}_k\cdot\vec{v}_i+\overline{\vec{\tau}_k\cdot\vec{v}_k}\rangle\!\rangle_a$, the following relation can be obtained

$$g_mh_{il}+q''_{il}=g_mh_{iv}+q''_{iv} \quad (22)$$

Assuming the saturation state at the interface, we obtain the relationship between the interfacial mass flux and heat flux.

$$g_m=\frac{q''_{il}-q''_{iv}}{h_{fg}} \quad (23)$$

As the interfacial heat flux in the gas phase, q''_{iv} is usually much smaller than q''_{il}, a simplified relationship can be obtained by neglecting q''_{iv}:

$$g_m=q''_{il}/h_{fg} \quad (24)$$

If we set up a physical model of q''_{il}, then mass

exchange rate can be obtained by using Eqs (21) and (24). Substituting Eq (24) into Eq (19), we have the interfacial energy transfer rate per unit volume,

$$Q_i=\frac{1}{L_a}\frac{q''_{il}h_g}{h_{fg}} \tag{25}$$

In addition to these conservative equations there are four equations of state:

$$\rho_v=\rho_v(p, T_v),\quad \rho_l=\rho_l(p, T_l)$$
$$e_v=e_v(p, T_v),\quad e_l=e_l(p, T_l) \tag{26}$$

These equations of state can be used to eliminate the densities and internal energies in terms of temperature and pressure. For the closure of the conservation equations terms, which represent the transfer of mass, energy, or momentum at the interface between the solid and fluid, and between liquid and vapor, must be explicitly expressed in terms of primary variables and properties. These terms are as follows:

$$\Gamma, \vec{F}_i, Q_i, \vec{F}_{wv}, \vec{F}_{wl}, Q_{wv}, \text{ and } Q_{wl}$$

The physical models of the above terms, so called constitutive equations, are described in Ref. 14.

3. Difference Equations of THERMIT-6S

The difference equations of THERMIT-6S are basically those of THERMIT (13) and can be obtained by discretizing the proceeding set of differential equations. The spatial discretization is characterized by a first-order spatial scheme, donor cell method, and staggered mesh layout. For time discretization a first-order semi-implicit scheme treats implicitly sonic terms and terms relating to local phenomena such as the exchange processes, and explicitly convective terms. A fully explicit method represents the fastest method on a per time step basis, but requires extremely small time steps due to Courant conditions. A implicit method, on the other hand, allows large time steps but leads to greatly increased code structure. The semi-

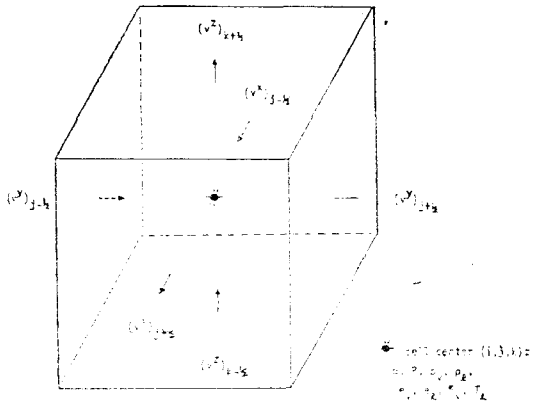

Fig. 1. A Typical Fluid Mesh Cell Showing Location of Variables and Subscripting Conventions

implicit method is a compromise between these two extremes; reasonable time step size but less computation time per time step and simpler code structure than the implicit method.

We begin with the mass and energy equations, which are differenced about the centers of the mesh cells. (See Fig. 1) The subscripts i, j, and k are used to indicate positions along the x, y, and z axes, respectively. The superscripts n or $n+1$ refers to the time level at which the variables are evaluated. A superscript $n+1/2$ is used only for the exchange terms which are functions of both new and old time values of variables. A and V represents the flow areas of the cell faces and the flow volumes of the cell, respectively. With these definition, the mass and energy difference equations are as follows:

Vapor Mass:

$$\frac{(\alpha_v\rho_v)^{n+1}-(\alpha_v\rho_v)^n}{\Delta t}$$
$$+\frac{1}{V}\{[A(\alpha_v\rho_v)^n(v_v^x)^{n+1}]_{i+1/2}$$
$$-[A(\alpha_v\rho_v)^n(v_v^x)^{n+1}]_{i-1/2}$$
$$+[A(\alpha_v\rho_v)^n(v_v^y)^{n+1}]_{j+1/2}$$
$$-[A(\alpha_v\rho_v)^n(v_v^y)^{n+1}]_{j-1/2}$$

$$+[A(\alpha_v\rho_v)^n(v_v^z)^{n+1}]_{k+1/2}$$

$$-[A(\alpha_v\rho_v)^n(v_v^z)^{n+1}]_{k-1/2}]=\Gamma^{n+1/2} \quad (27)$$

Liquid Mass:

Same as Eq. (27) with α_v replaced by α_l, subscript v by l and Γ by $-\Gamma$ (28)

Vapor Energy:

$$\frac{(\alpha_v\rho_v e_v)^{n+1}-(\alpha_v\rho_v e_v)^n}{\Delta t}$$

$$+\frac{1}{V}[A(\alpha_v\rho_v e_v+p)^n(v_v^x)^{n+1}]_{i+1/2}$$

$$-[A(\alpha_v\rho_v e_v+p)^n(v_v^x)^{n+1}]_{i-1/2}$$

$$+[A(\alpha_v\rho_v\rho_v+p)^n(v_v^y)^{n+1}]_{j+1/2}$$

$$-[A(\alpha_v\rho_v e_v+p)^n(v_v^y)^{n+1}]_{j-1/2}$$

$$+[A(\alpha_v\rho_v e_v+p)^n(v_v^z)^{n+1}]_{k+1/2}$$

$$-[A(\alpha_v\rho_v e_v+p)^n(v_v^z)^{n+1}]_{k-1/2}$$

$$+p^n\frac{\alpha^{n+1}{}_v-\alpha^n{}_v}{\Delta t}=Q_i^{n+1/2}+Q_{wl}^{n+1/2} \quad (29)$$

Liquid Energy:

Same as Eq. (29) with α_v replaced by α_l, subscript v by l and Q_i by $-Q_i$, and added Q_{ll} (30)

The liquid conduction term $\Delta\cdot\alpha_l(q_l+q_l')$ is expressed as Q_{ll} in Eq (30) and models for it is presented in Ref. 14. The properties transferred through the cell faces must be explicitly expressed in terms of cell centered quantities such as α, ρ_v, ρ_l, e_v and e_l. THERMIT-6S uses a particular relationship often referred to as donor-cell differencing; the properties will be transferred through the cell faces with all centered quantities upstream of that cell. If C stands for any cell-centered quantity, the value of $C_{i+1/2}$ is determined as

$$C_{i+1/2}=\begin{cases}C_{i+1} & \text{if } v_{i+1/2}^{n+1}\leq 0\\ C_i & \text{if } v_{i+1/2}^{n+1}\geq 0\end{cases} \quad (31)$$

For the donor cell decisions updated velocities are used. The primary reason to use updated velocities is to solve the packing problem which occurred if old velocities for donor-cell criteria were used.

Now let us consider only a single component of the vapor momentum. The additional equations are obtained by permutation of the axes and indices. According to the staggered mesh scheme, each momentum equation is differenced about the center of a face of a mesh cell. Based on Eq (14), the one-dimensional vapor momentum equation in the x direction is differenced at the point $(i+1/2, j, k)$ as follows:

$$(\alpha_v\rho_v+\alpha_v\rho_l C_v)_{i+1/2}^n\frac{(v_v{}^{xn+1}-v_v{}^{xn})_{i+1/2}}{\Delta t}$$

$$-(\alpha_v\rho_l C_v)_{i+1/2}^n\frac{(v_l{}^{xn+1}-v_l{}^{xn})_{i+1/2}}{\Delta t}$$

$$+E_{vi+1/2}^n+E_{vmi+1/2}^n$$

$$+\alpha_{v\,i+1/2}^n\frac{(p_{i+1}-p_i)^{n+1}}{\Delta x_{i+1/2}}$$

$$=K_u(v_v-v_l)_{i+1/2}^{n+1}-F_{wl}^{n+1/2}, \quad (32)$$

where

$$E_{vi+1/2}^n=(\alpha_v\rho_v)_{i+1/2}^n\Delta v_{vv}^n$$

$$E_{vmi+1/2}^n=(\alpha_v\rho_v C_v)_{i+1/2}^n[(\lambda-1)\Delta v_{vv}^n$$

$$-(\lambda-2)\Delta v_{lv}^n-\lambda\Delta v_{vl}^n-(1-\lambda)\Delta v_{ll}^n]$$

$$\Delta v_{vv}^n=v_{vvi+1/2}^x\left(\frac{\Delta_x v_v{}^x}{\Delta x}\right)_{1+1/2}v_{vi+1/2}^{yn}\left(\frac{\Delta_y v_v{}^x}{\Delta y}\right)_{i+1/2}^n$$

$$+v_{vi+1/2}^z\left(\frac{\Delta_z v_v{}^x}{\Delta z}\right)_{i+1/2}^n$$

$$\Delta v_{lv}^n=v_{li+1/2}^{x\,n}\left(\frac{\Delta_x v_v{}^x}{\Delta x}\right)_{i+1/2}^n+v_{li+1/2}^{y\,n}\left(\frac{\Delta_y v_v{}^x}{\Delta y}\right)_{i+1/2}^n$$

$$+v_{li+1/2}^z\left(\frac{\Delta_z v_v{}^x}{\Delta z}\right)_{i+1/2}^n$$

Δv_{vl}^n: same as Δv_{lv}^n with subscripts l replaced by v and v by l.

Δv_{ll}^n: same as Δv_{vv}^n with subscript v replaced by l.

In the above equation we have used an expression of the form $\frac{\Delta_x v_v{}^x}{\Delta x}$ to designate the difference approximation of $\frac{\partial v_v{}^x}{\partial x}$ associated with the point $(i+1/2, j, k)$. Similar expressions have been written for the y and z directions. In Eq

(32) we are again faced with the problem of variables appearing at locations other than those already defined. We first consider the quantity α:

$$\alpha_{i+1/2}=-\frac{\alpha_{i+1}\,\Delta x_{i+1}+\alpha_i\Delta x_i}{\Delta x_{i+1}+\Delta x_i} \tag{33}$$

The quantity $\rho_{vi+1/2}$ can be expressed in the same way as Eq (33). Every velocity except $v^x_{vi+1/2}$ is at the wrong position, so an averaging must be performed. We define

$$v^y_{vi+1/2}=\frac{1}{4}\left[v^y_{vi,j-1/2}+v^y_{vi,j+1/2}+v^y_{vi+1,j-1/2}+v^y_{vi+1,j+1/2}\right] \tag{34}$$

$$v^z_{vi+1/2}=\frac{1}{4}\left[v^z_{vi,k-1/2}+v^z_{vi,k+1/2}+v^z_{vi+1,k-1/2}+v^z_{vi+1,k+1/2}\right] \tag{35}$$

Finally, according to the donor cell scheme, the difference approximations of the convective derivatives are given by;

$$\left(\frac{\Delta_x v_v{}^x}{\Delta x}\right)_{i+1/2}=\begin{cases}\left(v^x_{vi+3/2}-v^x_{vi+1/2}\right)/\Delta x_{i+1} & \text{if } v^x_{vi+1/2}<0\\ \left(v^x_{vi+1/2}-v^x_{vi-1/2}\right)/\Delta x_i & \text{if } v^x_{vi+1/2}\geq 0\end{cases} \tag{36}$$

$$\left(\frac{\Delta_y v_v{}^x}{\Delta y}\right)_{i+1/2}=\begin{cases}\left(v^x_{vi+1/2,\,j+1}-v^x_{vi+1/2,j}\right)/\Delta y_{j+1/2} & \text{if } v^y_{vi+1/2}<0\\ \left(v^x_{vi+1/2,\,j}-v^x_{vi+1/2,\,j-1}\right)/\Delta y_{j-1/2} & \text{if } v^y_{vi+1/2}\geq 0\end{cases} \tag{37}$$

$$\left(\frac{\Delta_z v_v{}^x}{\Delta z}\right)_{i+1/2}=\begin{cases}\left(v^x_{vi+1/2,\,k+1}-v^x_{vi+1/2,k}\right)/\Delta z_{k+1/2} & \text{if } v^z_{vi+1/2}<0\\ \left(v^x_{vi+1/2,\,k}-v^x_{vi+1/2,\,k-1}\right)/\Delta z_{k-1/2} & \text{if } v^z_{vi+1/2}\geq 0\end{cases} \tag{38}$$

The mesh spacings $\Delta y_{j+1/2}$ and $\Delta z_{k+1/2}$ appearing in the above expressions are evaluated as;

$$\Delta y_{j+1/2}=(\Delta y_j+\Delta y_{j+1})/2 \tag{39}$$

$$\Delta z_{k+1/2}=(\Delta z_k+\Delta z_{k+1})/2 \tag{40}$$

We have now completed our specification of the difference equations, with the exception of the exchange terms. These terms are discussed in Ref. 14.

4. Solution Procedure of THERMIT-6S

The most important characteristic of our difference equations lies in the treatment of coupling terms. An examination of the mass and energy equations reveals that cell-centered variables appering in these equations such as α^{n+1}, p^{n+1}, and e^{n+1} are coupled only to the new-time velocities v^{n+1} on the faces of the mesh cell. The momentum equation relates these velocities only to the pressure in the mesh cell in question and in the six surrounding cells. Thus we see that coupling between mesh cells at time level $n+1$ is through the pressure variable. Hence, we need to solve only the reduced pressure equation.

Let us describe how this is accomplished. Denote the system of two-fluid finite difference equations by $F(x)=0$. Here, x is a vector containing the ten principal unknow variables. We shall use a Newton iteration to solve the non-linear system,

$$F(x)=0 \tag{41}$$

We first linearize the old iterate x^m as

$$F(x)\cong F(x^{m+1})=F(x^m)+J(x^m)\,(x^{m+1}-x^m)=0 \tag{42}$$

where the Jacobian matrix $J(x^m)$ is defined as $\left(\frac{\partial F}{\partial x}\right)^m_x$ We then solve the following linear system for

$$J(x^m)\Delta x^{m+1}=-F(x^m) \tag{43}$$

where Δx^{m+1} is the iteration error $(x^{m+1}-x^m)$ and $F(x^m)$ is called a residual error.

This linear system is solved either by the direct method or iteration method. This process is called as the inner iteration. This Newton

iteration, called as the outer iteration, continues until the iteration error Δx^{m+1} or the residual error $F(x^m)$ is sufficiently small.

The first procedure is to express velocities in the momentum equations in terms of pressure. Because the interfacial momentum exchange term has been treated implicity, the liquid and vapor velocities are coupled with each other. At the face of each mesh cell, the momentum equations can be put in the form

$$\begin{bmatrix} x & x \\ x & x \end{bmatrix} \begin{bmatrix} v_v^{m+1} \\ v_l^{m+1} \end{bmatrix} = \begin{bmatrix} a\Delta p^{m+1}+f \\ b\Delta p^{m+1}+g \end{bmatrix} \tag{44}$$

By solvingthe above 2×2 matrix, we determine each velocity in terms of the pressure difference as

$$v_v^{m+1}=c\Delta p^{m+1}+f'$$
$$v_l^{m+1}=d\Delta p^{m+1}+g' \tag{45}$$

The above equations can now be used to eliminate all velocities appearing in the mass and enery. Then we finally obtain a set of four equations for each mesh cell involving the four unknowns, p, α, T_v, and T_l, at the center of the mesh cells and pressures, at the centers of the six adjacent cells.

$$\begin{bmatrix} x & x & x & x \\ x & x & x & x \\ x & x & x & x \\ x & x & x & x \end{bmatrix} \begin{bmatrix} p \\ \alpha \\ T_v \\ T_l \end{bmatrix} + \begin{bmatrix} x & x & x & x & x & x \\ x & x & x & x & x & x \\ x & x & x & x & x & x \\ x & x & x & x & x & x \end{bmatrix} \begin{bmatrix} p_1 \\ \vdots \\ p_6 \end{bmatrix} = \begin{bmatrix} x \\ x \\ x \\ x \end{bmatrix} \tag{46}$$

By inverting the 4×4 matrix that appears above, we can put this system in the reduced form:

$$\begin{bmatrix} | & & & 0 \\ & | & & \\ & & | & \\ 0 & & & | \end{bmatrix} \begin{bmatrix} p \\ \alpha \\ T_v \\ T_l \end{bmatrix} + \begin{bmatrix} x & x & x & x & x & x \\ x & x & x & x & x & x \\ x & x & x & x & x & x \\ x & x & x & x & x & x \end{bmatrix} \begin{bmatrix} p_1 \\ \vdots \\ p_6 \end{bmatrix} = \begin{bmatrix} x \\ x \\ x \\ x \end{bmatrix} \tag{47}$$

The first equation in the above set is an equation involving only the pressure in a cell and its six neighbors. The remaining three equations relate the void fraction and temperature to the pressure. The pressure equation can be solved iteratively with each complete sweep referred to as an inner iteration. Once the pressure field is found, the other unknowns α, T_v, and T_l can be found by back substitution. The above procedure is repeated until the pressure iteration error, Δp^{m+1} is sufficiently small. If convergence is not attained in a specified number of iterations, the time step size is reduced and the same procedure is repeated. The method will always converge, if the time step size is small enough.

A crucial property of the reduced pressure problem is its diagonal dominance. In the one-dimensional flow the pressure equations can be expressed as follows:

$$p_{i+1}^{m+1}-\left[2+\left(\frac{a^{-1}\,\Delta x}{\Delta t}\right)^2\right]p_i^{m+1}+p_{i-1}^{m+1}=\cdots$$

where a is the sound speed

$$a^{-2}=\left(\frac{\partial\rho}{\partial p}\right)_p$$

The amount by which the sum of any row of coefficients exceeds zero can always be expressed in the form $\left(\frac{a^{-1}\Delta x}{\Delta t}\right)^2$.

5. Numerical Simulation

OPERA is an Out-of-Pile expulsion and Reentry Apparatus at ANL. OPERA 15-Pin (15) is a sodium experiment which simulates the initiating phase of a pump coastdown without the scram of a LMFBR, specifically, the FFTF. The objective of the OPERA 15-Pin pump-coastdown test is to investigate sodium boiling initiation and the subsequent two-dimensional nature of sodium voiding in large pin

bundles approaching the size of current LMFBR subassemblies. In a large pin bundle the steep radial coolant temperature profile will affect the behavior of vapor generation, vapor condensation, onset of flow reversal, radial voiding, clad dryout, and the axial void oscillations.

This experiment utilized 15 electric fuel pin simulators in a triangular thin walled duct to represent a high powered sub-assembly in which each pin produces 33 Kw. The 15-Pin triangular test bundle was fabricated to simulate the one-sixth sector of a 61-pin hexagonal bundle.

The OPERA facility is a once-through sodium system. Steady-state coolant flow with the inlet temperature 588 K through the test section is generated by first pressurizing the blowdown vessel with argon gas, opening the sodium control valves at the inlet to the test section, and at the same time venting the receiver vessel to atmosphere. The pump-coastdown flow transient is generated by depressurizing the blowdown vessel through a valve and two nozzles, which can be preset by calibration procedures, to give the desired flow decay. The summary of OPERA 15-pin test is given in Table 1.

The pin power is maintained at 33 Kw until 3 heater pins fail or their power output varies 10% from the full 33 Kw at which time all pin power is terminated.

Full size wire wraps (0.0142cm O.D.) are on the interior pins and the pins on the one side of bundle where the outside wall conditions are to be simulated. Small wire wraps (0.079cm O.D.) and fillers (0.158cm O.D.) are used on the pins and walls at the other two sides of the bundle where the interior part of the 61-pin bundle is to be simulated. This arrangement ensures that the power to flow ratio of each subchannel is the same as the corresponding subchannel in a 61-Pin hexagonal bundle. The thermal capacitance of the wall is minimized by using a thin wall of 0.5mm thickness.

Table 1 Summary of OPERA 15-Pin Test

Coolant Inlet Temperature	323°C
Coolant Velocity in Test Bundle	4.28m/sec
Average Pin Power	26.7Kw
Test Bundle Inlet Pressure	0.315MPa
Test Bundle Outlet Pressure	0.200MPa
Fuel Diameter (O.D)	0.584cm
Full Length 226cm	226cm
Length of Heated Zone	91.4cm
Length of Plenum Region	121.9cm

A 2-D analysis is performed for the OPERA-15 Pin numerical simulation. The test section consists of five mesh zones in the radial direction. Twenty nine mesh zones in the axial direction are considered: 18 in the heated section (each 2″) and 11 in the unheated section (each 2″ for low 3 mesh zones and each 6″ for the next 8 mesh zones).

Inlet and outlet boundaries are positioned at the outlet of the blowdown vessel and inlet of the receiver vessel, respectively. As the receiver vessel is connected to the atmosphere, the outlet pressure is set to be equal to one atmosphere over the transients. The inlet velocities measured in the experiment are used for the inlet boundary condition up to 9 seconds into the OPERA-15 Pin flow transients when boiling starts in the numerical simulation. After boiling the outlet pressure estimated by the figure of blowdown vessel depressurization given in Ref (15) is used for the outlet boundary condition. Uniform radial and axial power distributions, and constant Nusselt number for liquid heat conduction, Nu=22, are used.

The results by the present code were obtained by using the pretest information package for the OPERA-15 Pin, which contains only experiment apparatus, test section description, and operating proceduresfore. Therefore it is interesting to compare predictions by the present code to experimental data (16) which were published later.

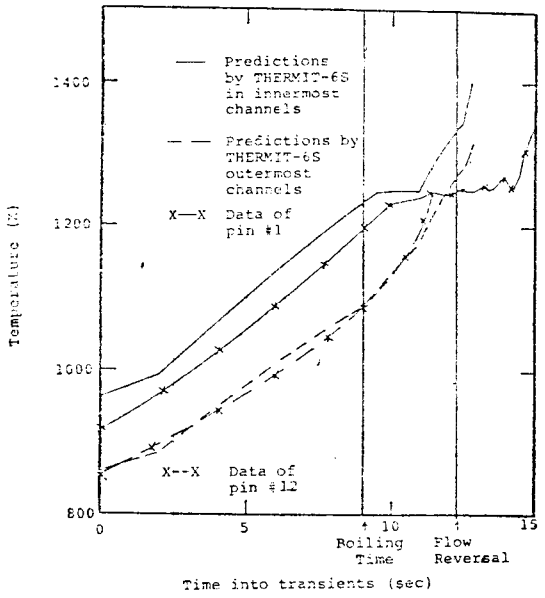

Fig. 2. Comparison of Temperature Transients of OPERA-15 Pin with Pretest Predictions by THERMIT-6S at 35.5″ (above fuel bottom) in Innermost and Outermost Channels.

Boiling first starts at 9 seconds into transients in the hottest channel, compared to 9.4 seconds in the test. Fig. 2. illustrates one of the primary reasons for the prediction of this earlier boiling: temperature predicted by the present code is higher than data over transients.

Up to 2 seconds after boiling starts, flow coastdown is very slow. Figgures 3 and 4 reveal the reason of this slow flow coastdown: it takes about 1.8 seconds for vapor to reach the outer most channel due to the large bundle size, large inlet hydraulic resistance, and large radial temperature gradients. In the test it was estimated that the sodium void progresses from the innermost channel to the outermost channel in about 1.5 seconds.

Rapid flow coastdown follows and flow reversal at the inlet occurs at 3.1 seconds from incipient boiling, compared to 2.6 seconds in the experiment. (see Fig. 5) This delay of flow reversal is attributed to larger temperature drop

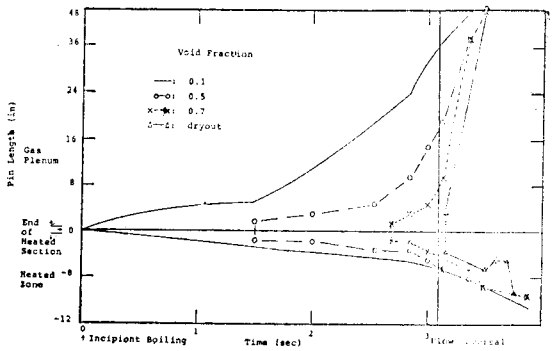

Fig. 3. Axial Void Profile in Innermost Channel Predicted by THERMIT-6S for the OPERA-15 Pin Test

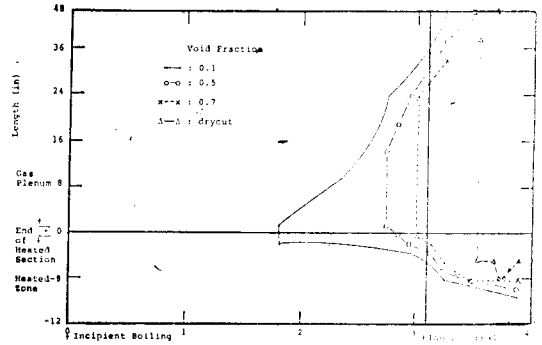

Fig. 4. Axial Void Profile in Outermost Channel Predicted by THERMIT-6S for the OPERA-15 Pin Test

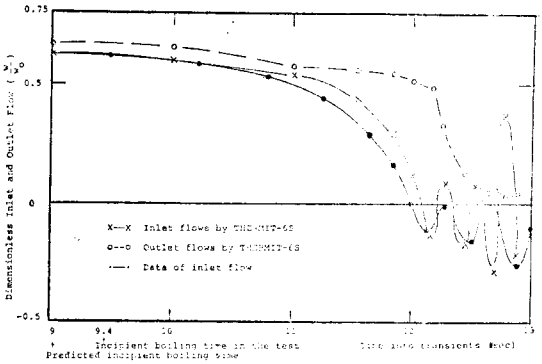

Fig. 5. Comparison of Flow Transients of OPERA-15 Pin with Pretest Predictions by THERMIT-6S

laterally across the bundle in the computation which is 144 K at boiling inception, compared to 109 K in the experiment. Note that for all three experiments simulating the low flow/high

power accidents, rapid flow coastdown occured when the outmost channel reaches around saturation temperature and vapor production in some cells of the outmost channel takes place instead of vapor condensation.

The outlet flow is almost constant up to 3.2 seconds when vapor reaches the end of the test section. Afterwards, the outlet flow rapidly drops due to high void fraction at the end of the test section, but never becomes the negative flow because the interfacial force by high vapor velocities drags the liquid along.

Within 0.05 seconds after flow reversal, dryout is predicted. However, the occurrence of dryout in the experiment was substantially delayed; elasped time from inlet flow reversal to dryout is around 2 seconds. In the computation liquid reentry occurs at 0.14 seconds after flow reversal and is followed by inlet flow oscillation of which the frequency is 3.5 cycles/sec, compared to 2 cycles/sec in the experiment.

6. Conclusion

THERMIT-6S with the proposed two-fluid differential equations, finite difference model, and solution scheme were used to simulate the OPERA-15 experiment. THERMIT-6S was found to be a very powerful tool in predicting reactor behavior after sodium boiling including flow coastdown, reversal flow, and flow oscillation.

References

1. R.C. Noyes, J.G. Morgan, and H.H. Cappel, "Transfugue-I, A Digital Code for Transient Two-Phase Flow and Heat Transfer", NAA-SR-11008 (1965)
2. J.E. Meyer, "Hydrodynamic Models for the Treatment of Reactor Thermal Transients," Nucl. Sci. Eng., 10(1961).
3. D.R. MacFarlane, Ed., "SASIA, A Computer Code for the Analysis of Fast Reactor Power and Flow Transients," ANL-7607 (1970).
4. J.A. Landomi, "Transfugue -IIa A Digital Code for Transient Two-Phase Flow in Single Heated Channels," NAA-SR-12503 (1968).
5. F.E. Dunn et al., "The SAS2A Accident Analysis Computer Code," ANL-8138 (1975).
6. M.G. Stevenson et al., "Current Status and Experimental Basis of the SAS LMFBR Accident Analysis Code System," USAEC-CONF 740401 (1974).
7. J.E. Cahalan et al., "SAS3D LMFBR Accident Analysis Computer Code,"
8. J.E. Cahalan et al., "The Status and Experimental Basis of the SAS4A Accident Analysis Code System," Proc. Int. Mtg. on Fast Reactor Safety Technoloyg, Seattle, Vol. II. (1979).
9. P. Wirtz, "Ein Beitrag zur Theoretischen Beschreibung des Siedens Unter Storfallbedingungen in natriumgekuhlten Schnellen Seaktoren," KFK 1858 (1973).
10. W.W. Marr, "COBRA-3M: A Digital Computer Code for Analyzing Thermal Hydraulic Behaivor in Pin Bundles." ANL-8131 (1975).
11. C.W. Stewart et al., "COBRA-IV: The Model and the Method," BNWL-2214, NRC-4 (1977).
12. G. Basque et al., "Theoretical Analysis and Experimental Evidence of Three Types of Thermohydraulic Incoherency in Undisturbed Cluster Geometry," IAEA Specialists Meeting, Karlsrule (1979).
13. W.H. Reed and H.B. Stewart, "THERMIT-A Computer Program for Three-Dimensional Thermal Hydraulic Analysis of Light Water Reactors Codes," M.I.T.
14. Hee Cheon No, "General Derivation of Two-Fluid Model," J. of the Korean Nuclear Society, V. 16, No. 1, (1984).
15. T.J. Scale. "Pretest Information Package for OPERA 15-Pin Experiment," ANL/RAS 81-32, (1981).
16. T.J. Scale et al., "OPERA 15-Pin Sodium Expulsion Test," ANS Trans., Vol. 43 (1982).